Flotillin mediated membrane fluidity controls peptidoglycan synthesis and MreB movement.

Aleksandra Zielińska[#,1], Abigail Savietto[#,2,8], Anabela de Sousa Borges[1], Denis Martinez[3], Melanie Berbon[3], Joël R. Roelofsen[1], Alwin M. Hartman[4,5,6], Rinse de Boer[7], Ida J. van der Klei[6], Anna K. H. Hirsch[4,5,6], Birgit Habenstein[3], Marc Bramkamp[*,2,8], Dirk-Jan Scheffers[*,1]

[#]equal contribution; [*]corresponding author

[1]Molecular Microbiology, Groningen Biomolecular Sciences and Biotechnology Institute, University of Groningen, the Netherlands; [2]Biozentrum, Ludwig-Maximilians-Universität München, Germany; [3] Institute of Chemistry & Biology of Membranes & Nanoobjects (UMR5248 CBMN), IECB, CNRS, Université Bordeaux, Institut Polytechnique Bordeaux, Pessac, France; [4]Department of Drug Design and Optimization (DDOP), Helmholtz-Institute for Pharmaceutical Research Saarland (HIPS) - Helmholtz Centre for Infection Research (HZI), Saarbrücken, Germany; [5]Department of Pharmacy, Saarland University, Saarbrücken, Germany; [6]Stratingh Institute for Chemistry, University of Groningen, The Netherlands; [7]Molecular Cell Biology, Groningen Biomolecular Sciences and Biotechnology Institute, University of Groningen, the Netherlands. [8]Institute for General Microbiology, Christian-Albrechts-University Kiel, Germany.

[*]correspondence: marc.bramkamp@lmu.de; d.j.scheffers@rug.nl

Abstract

The bacterial plasma membrane is an important cellular compartment. In recent years it has become obvious that protein complexes and lipids are not uniformly distributed within membranes. Current hypotheses suggest that flotillin proteins are required for the formation of complexes of membrane proteins including cell-wall synthetic proteins. We show here that bacterial flotillins are important factors for membrane fluidity homeostasis. Loss of flotillins leads to a decrease in membrane fluidity that in turn leads to alterations in MreB dynamics and, as a consequence, in peptidoglycan synthesis. These alterations are reverted when membrane fluidity is restored by a chemical fluidizer. *In*

29 ***vitro*, the addition of a flotillin increases membrane fluidity of liposomes. Our data**
30 **support a model in which flotillins are required for direct control of membrane fluidity**
31 **rather than for the formation of protein complexes via direct protein-protein interactions.**
32

33 **Introduction**

34 The shape of a bacterium is predominantly defined by the structure of its peptidoglycan.
35 Although there is a great variety in bacterial shapes, the overall chemistry of peptidoglycan is
36 very similar between bacteria and thus the shape of peptidoglycan is primarily determined by
37 the temporal and spatial regulation of peptidoglycan synthesis. In rod-shaped bacteria,
38 peptidoglycan synthesis is thought to be mediated by two protein assemblies, the elongasome
39 and the divisome, that synthesize peptidoglycan along the long axis and across the division
40 plane of the cell, respectively[1,2]. These complexes contain a set of proteins required for the
41 final steps of synthesis and translocation of the peptidoglycan precursor, LipidII, from the inner
42 to the outer leaflet of the cytoplasmic membrane, and proteins that incorporate LipidII into
43 peptidoglycan. These include SEDS (Shape, Elongation, Division and Sporulation) proteins
44 that can perform glycosyl transferase reactions[3-5], and Penicillin Binding Proteins (PBPs) that
45 are divided in class A PBPs (aPBPs) that catalyse both glycosyl transferase and transpeptidase
46 reactions, class B PBPs (bPBPs) that only catalyse transpeptidase reactions and low molecular
47 weight PBPs that modify peptidoglycan, as well as hydrolases[2,6].
48 Coordination of these complexes is linked to cytoskeletal elements, MreB (-like proteins) for
49 the elongasome and FtsZ for the divisome. In models, the cytoplasmic membrane is often
50 depicted as a passive environment in which these machineries are embedded. However, it is
51 becoming clear that the structure of the membrane plays a critical role in the coordination of
52 peptidoglycan synthesis[7]. Inward membrane curvature serves as a localization trigger for MreB
53 and the elongasome, and enhanced local synthesis at bulges straightens out the membrane

54 sufficient to convert spherical cells to a rod shape[8,9]. In *Bacillus subtilis,* the motion of MreB
55 along the membrane is associated with elongasome activity[10,11] and the velocity of MreB
56 patches is related to growth rate[12], indicating that MreB motion can be used as a marker for
57 elongasome activity. Interestingly, MreB localizes to and organizes regions of increased
58 membrane fluidity (RIF)[13], which in turn is linked to the presence of LipidII, which favours a
59 more fluid membrane and promotes local membrane disorder[14,15]. Inhibition of LipidII
60 synthesis by genetic or chemical means results in a dissolution of membrane structures
61 observed with the dye FM 4-64 and release of MreB from the membrane[10,11,16,17].
62 Next to RIFs, membrane regions of decreased fluidity have been identified in bacteria[7,18,19].
63 These so-called functional membrane microdomains (FMMs) are thought to be organized by
64 the bacterial flotillin proteins, are enriched in isoprenoid lipids [20,21], and can be found in so-
65 called Detergent Resistant Membrane (DRM) fractions of the membrane. Since the formulation
66 of the FMM hypothesis, FMMs have been linked to many processes, such as protein secretion,
67 biofilm formation, competence and cell morphology[22-25]. Cell morphology effects are linked
68 to cell wall synthesis, and analysis of the protein content of *Bacillus subtilis* DRMs identified
69 several PBPs, MreC and other proteins involved in cell wall metabolism as well as the two
70 flotillins, FloA and FloT[21,24,26]. FloA is constitutively expressed, whereas FloT is expressed
71 primarily during stationary growth, cell wall stress and sporulation [27-29]. Super resolution
72 microscopy showed that the flotillins and other proteins found in DRMs do not colocalize and
73 have different dynamics[30], so it is unlikely that FMMs are regions in the membrane that offer
74 a favourable environment in which these membrane proteins are continuously present and
75 active. Recently, the hypothesis has been put forward that FMMs/flotillins form a platform for
76 the formation of functional protein oligomers, as work in *Staphylococcus aureus* showed that
77 multimerization of Type 7 secretion systems and PBP2a depends on FMMs[19,20,31].

78 Here, we have analysed the role of flotillins in peptidoglycan synthesis in *B. subtilis.* Our
79 results show that, at high growth rates, flotillins control membrane fluidity in a manner that is
80 critical for peptidoglycan synthesis and MreB dynamics, but have no effect on PBP
81 oligomerization. This results in a new model for flotillin function in the physical organization
82 of membranes during fast growth in rich medium.
83
84 **Results**
85 *Absence of flotillins shifts peptidoglycan synthesis to division septa*

86 In previous studies, a double deletion of *floA/floT* was either reported to suffer severe shape
87 defects and perturbed membrane structure[25], or to not have strong shape defects but with a
88 change in the overall lipid ordering of the membrane[24]. We grew wild type and Δ*floAT* strains
89 and analysed exponentially growing cells. We did not observe striking shape defects, but did
90 see an increase in median cell length and distribution of cell lengths in the absence of flotillins
91 (**Figure 1A, G**). To look at effects on peptidoglycan synthesis, we labelled cells with HADA,
92 a fluorescent D-Alanine analogue that reports on sites of active peptidoglycan synthesis[32], and
93 with fluorescent vancomycin (Van-FL), which labels LipidII and peptidoglycan containing
94 pentapeptide side chains[33,34]. This revealed a significant accumulation of peptidoglycan
95 synthesis stains at division septa in the Δ*floAT* strain (**Figure 1A-C**). To look at membrane
96 structure, cells were labelled with FM4-64, Nile-Red and DiI-C12, which are lipid dyes that
97 accumulate in zones enriched in fluid lipids[13]. Again, the stains accumulated at the septa in the
98 Δ*floAT* strain, which also showed some accumulation of FM4-64 and DiI-C12 in patches,
99 suggesting that the more fluid regions of the membrane are coalescing into larger regions
100 (**Figure 1A, D-F**). The HADA, FM4-64 and Nile-Red measurements were repeated using a
101 wild type strain expressing endogenous GFP, allowing simultaneous imaging of both strains
102 on the same slide, and gave similar results, confirming that the observed signal increase is not

103 due to variation between microcopy experiments (**Figure 1 - figure supplement 1 A,B**). In
104 this mixed-strain experiment, Nile-Red labelling at the lateral membrane was the same between
105 wild type and Δ*floAT* strains, indicating that there is no difference in dye diffusion between the
106 strains (**Figure 1 - figure supplement 1D**). Inspection of the septa by electron microscopy
107 revealed that there was no difference between the thicknesses of the septa between the wild
108 type and Δ*floAT* strain, ruling out that the increase in signal was due to formation of thicker
109 septa (**Figure 1 - figure supplement 1C**). The shift of peptidoglycan synthesis to the division
110 site could hint at stress in the overall peptidoglycan synthesis route. This was confirmed by
111 growing cells at a sublethal concentration of fosfomycin, which limits synthesis of LipidII[35],
112 but that does not impact growth rate at the concentration used. This resulted in bulging cells
113 and some lysis, which was exacerbated in the Δ*floAT* strain (**Figure 1 - figure supplement**
114 **1F,G**). It should be noted that the peptidoglycan synthesis stress caused by fosfomycin is not
115 the same as the stress caused by the absence of flotillins, as the phenotypes of wild type cells
116 with sublethal fosfomycin are quite distinct from Δ*floAT* cells without fosfomycin.

117 We ruled out that the peptidoglycan synthesis stress was caused by a change in the folding or
118 complex formation by PBPs in the absence of flotillins, as there were no differences in the
119 overall PBP-profiles of Bocillin-FL labelled wild type or flotillin deletion strains (**Figure 1 -**
120 **figure supplement 2A**). PBP complex formation was analysed by analysis of Bocillin-labelled
121 membrane fractions using a combination of Native-PAGE and SDS-PAGE[36] and showed that
122 various PBPs can be found in a high-MW complex (notably PBPs 1, 2, 3 and 4), but that
123 complex formation is similar in the Δ*floAT* strain (**Figure 1 - figure supplement 2B**). Also,
124 none of the five functional GFP-PBPs examined changed their localization in the Δ*floAT* strain
125 (**Figure 1 - figure supplement 2C**). Overall, the data suggest that in the absence of flotillins,

126 peptidoglycan synthesis is affected and relatively increased at division septa, with a

127 concomitant accumulation of membrane dyes that are indicative of higher membrane fluidity.

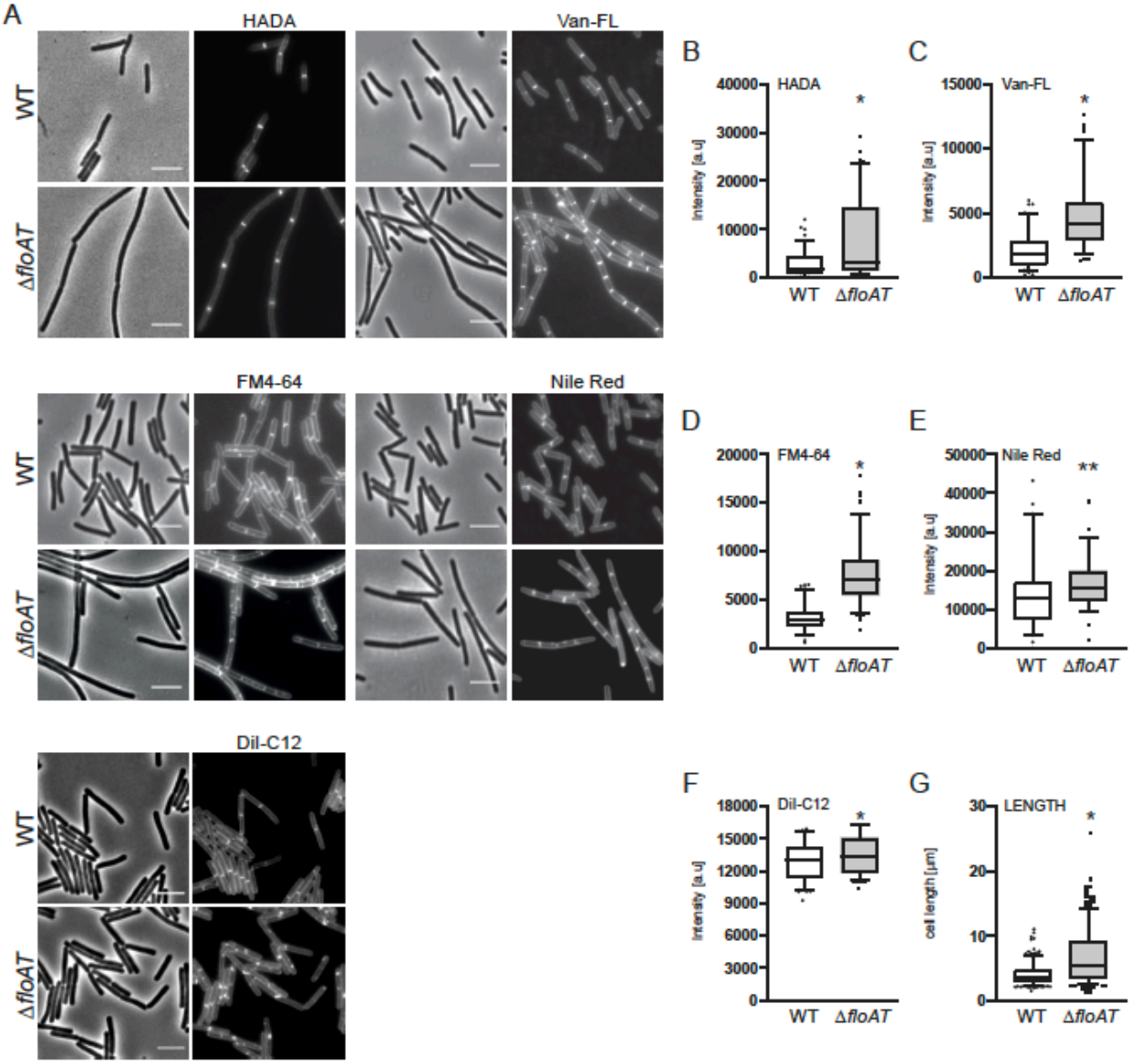

128

129 **Figure 1. Accumulation of peptidoglycan synthesis and membrane material at division**

130 **sites in a flotillin mutant. A**. Morphology of the exponentially growing wild type (WT) and

131 Δ*floAT* strains labelled with HADA, fluorescent Vancomycin (Van-FL), FM 4-64, Nile Red,

132 and DiI-C12. Scale bar 5 µm. **B-F**. Peak intensity of HADA (B), Van-FL (C), Nile Red (D),

133 FM4-64 (E) and DiI-C12 (F) labelled division sites of the cells shown in (A). Cells from each

134 strain (n ≥ 100, except E, n = 60) were analysed using the ObjectJ macro tool PeakFinder. **G**.
135 Distribution of the cell length (n = 100) of the strains analyzed in (A).
136 All data analysed with Prism and depicted as box plots with whiskers indicating 5-95%
137 percentile. Significant differences are based on the two-tailed Mann-Whitney test (* $p<0.05$;
138 ** $p<0.01$).
139

140 *The absence of both flotillins and PBP1 causes a severe phenotype, linked to a loss of*
141 *membrane fluidity.*
142 We reasoned that a non-lethal defect in septal peptidoglycan synthesis could reveal more about
143 the role of flotillins and constructed a flotillin mutant that lacks PBP1, a bifunctional glycosyl
144 transferase/transpeptidase that is required for efficient cell division[37]. Simultaneous deletion of
145 *pbp1*, *floA*, and *floT* resulted in strong filamentation and delocalization of peptidoglycan
146 synthesis as well as membrane dyes to patches **(Figure 2A, Figure 2 - figure supplement 1A)**.
147 Deletion of single flotillin genes and PBP1 had similar, albeit less severe effects **(Figure 2 -**
148 **figure supplement 1B, C)**. To exclude the possibility that an alteration of peptidoglycan
149 modification resulted in the delocalization of HADA and Van-FL, we used D-Alanine-D-
150 Propargylglycine (D-Ala-D-Pra), a clickable dipeptide analogue which is exclusively
151 incorporated into peptidoglycan via LipidII[38]. D-Ala-D-Pra incorporation was delocalized in
152 the Δ*pbp1ΔfloAT* strain, indicating that peptidoglycan synthesis itself is delocalized (**Figure 2**
153 **- figure supplement 1D**). So far, our experiments were done with fast growing cells and
154 Lysogeny Broth (LB) as the growth medium. Strikingly, none of the mutant strains had an
155 apparent phenotype when cultivated in Spizizen's minimal medium (SMM, **Figure 2B**), and
156 peptidoglycan synthesis and lipid dyes were no longer accumulating at division sites in the
157 Δ*floAT* strain (**Figure 2 - figure supplement 2**). SMM has a higher Mg^{2+} concentration, which
158 is known to rescue various cell shape mutations by inhibition of cell wall hydrolysis[39].

159 However, the increase in Mg^{2+} was not sufficient to explain the reversal of phenotype as cells
160 grown on LB supplemented with Mg^{2+} (6 mM, concentration in SMM, or 20 mM) still
161 displayed the elongated phenotype with delocalized peptidoglycan synthesis **(Figure 2 - figure**
162 **supplement 3)**. This indicated that the phenotypes associated with the absence of flotillins are
163 growth-rate and/or nutrient related.
164

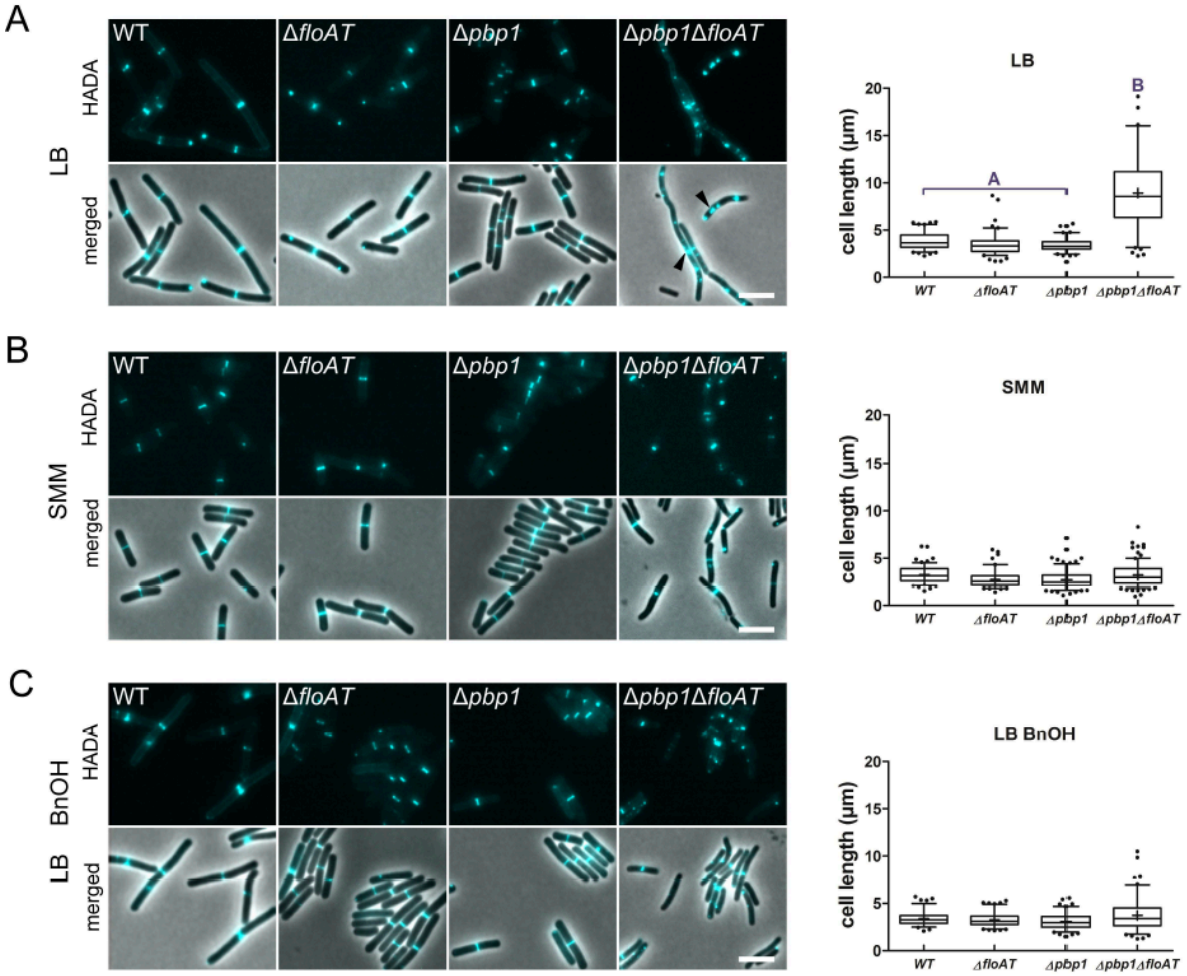

165

166 **Figure 2. Cell morphology and cell wall synthesis localization is dependent on growth**
167 **conditions.** Morphology of the *WT*, Δ*floAT*, Δ*pbp1*, and Δ*pbp1*Δ*floAT* strains grown in **(A)**
168 rich (LB), **(B)** minimal (SMM) medium, and in **(C)** rich medium with membrane fluidizing
169 conditions (0.1 % benzyl alcohol, LB BnOH). Cells were labelled with HADA, and aberrant
170 cell shape and peptidoglycan synthesis are indicated with arrowheads. Panels on the right
171 indicate corresponding cell length distributions (n ≥ 100). Distributions were analysed using
172 Dunn's multiple comparison tests after Kruskal–Wallis. Statistically significant cell length

173 distribution classes ($p < 0.001$) are represented as letters above each graph – in B and C there
174 were no significant differences. Whiskers represent 5-95% percentile, "+" represent the means
175 Scale bar: 4 µm.

176

177 Next, we determined lipid packing order in the different strains using the fluorescent dye
178 Laurdan, a reporter for flotillin-mediated lipid ordering[24]. LB-grown cells lacking flotillins
179 displayed an increased generalized polarization (GP)[24], indicative of an overall increase in
180 ordered lipid packing in the membrane, but the effect of flotillins on membrane ordering
181 completely disappeared when cells were grown on SMM **(Figure 3)**. The resolution obtained
182 with Laurdan does not allow the detection of local differences in fluidity between the lateral
183 membrane and the septa, but does report on overall lipid ordering. Overall, lipid order was
184 increased in cells grown on SMM compared to LB **(Figure 3)**, whereas the absence of PBP1
185 had no significant effect on membrane fluidity, also not when combined with flotillin deletions
186 **(Figure 3)**. The changes in lipid ordering were not due to changes in the overall fatty acid
187 composition of the membranes - the ratios of C17/C15 side chains and *iso/anteiso* fatty acids,
188 which are indicative of fluidity[13], were identical for wild type and Δ*floAT* strains grown on LB,
189 and very similar for cells grown on SMM (**Figure 3 - figure supplement 1**).

190

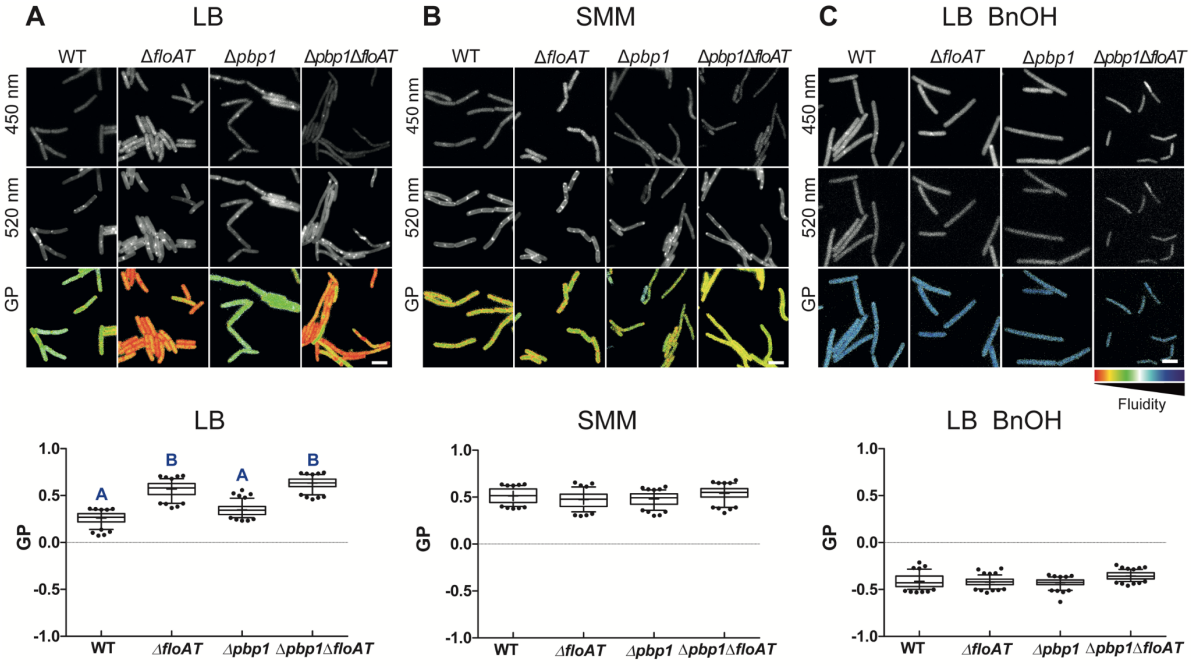

Figure 3. Flotillins increase overall membrane fluidity at high growth rate. Changes in overall membrane fluidity were assessed by Laurdan microscopy in cells grown on LB (**A**), SMM (**B**) and LB+BnOH (**C**). Micrographs show colour-coded generalized polarization (GP) maps in which red indicates regions of decreased fluidity (scale bar: 4 µm). Correspondent theoretical GP measurements in the graphs vary from -1 (more fluid) to 1 (less fluid). Significant statistical differences according to Dunn's multiple comparison tests after Kruskal–Wallis are represented as letters above each graph in panel **A**. Datasets labeled as A are significantly different from datasets labeled as B; datasets with the same letter are not significantly different. No statistically significant difference was observed for the data in panels **B** and **C** ($p < 0.001$; $n \geq 150$, two biological replicates).

Restoring membrane fluidity rescues normal peptidoglycan synthesis.

The GP values indicated that membranes are more ordered when cells are grown on minimal medium, and this suggests that the flotillin-associated increase in overall membrane fluidity is important for cell shape control at high growth rates. This was tested by growing the strains lacking flotillins and PBP1 on LB in the presence of benzyl alcohol, an extensively used membrane fluidizer that increases membrane hydration due to disordering of membrane

209 structure[40]. Notably, the addition of benzyl alcohol increased membrane fluidity to similar
210 extents in the wild type and the mutant strains (see Figure 3C), but did not affect the growth
211 rates of the strains (**Figure 2 – figure supplement 4**). The increase in membrane fluidity
212 restored normal cell length and normal peptidoglycan synthesis patterns to the *pbp1*/*floA*/*floT*
213 strain **(Figure 2C)**.
214 In *B. subtilis*, the rate of growth and of peptidoglycan synthesis is linked to the speed of MreB
215 movement – in minimal media, the speed of MreB patches is reduced compared to the speed
216 in rich media[12]. Analysis of the movement of a fully functional mRFPruby-MreB fusion[10] by
217 time lapse TIRF (Total Internal Reflection Fluorescence) microscopy, confirmed that MreB
218 patch mobility is higher in cells grown on LB than in cells grown on SMM, with MreB speeds
219 similar to those reported previously[12] **(Figure 4, supplemental movie 1, 2)**. Strikingly, in the
220 absence of flotillins, MreB patch mobility was notably decreased in cells grown on LB, while
221 in SMM grown cells MreB patch mobility was independent of the presence of flotillins (**Figure**
222 **4, supplemental movie 3,4**). Fluidizing the membrane with benzyl alcohol, which does not
223 alter the growth rate, almost completely restored MreB mobility in LB grown cells **(Figure 4,**
224 **supplemental movie 5, 6)**. These results indicate that the MreB patch mobility is not only
225 controlled by growth rate but also by membrane fluidity. Thus, in fast growing cells with
226 decreased membrane fluidity there is a decrease in elongasome mediated peptidoglycan
227 synthesis, reflected by the reduction of MreB mobility. This fits with an observed increase in
228 peptidoglycan synthesis at the division site, which may act as a compensatory mechanism.
229

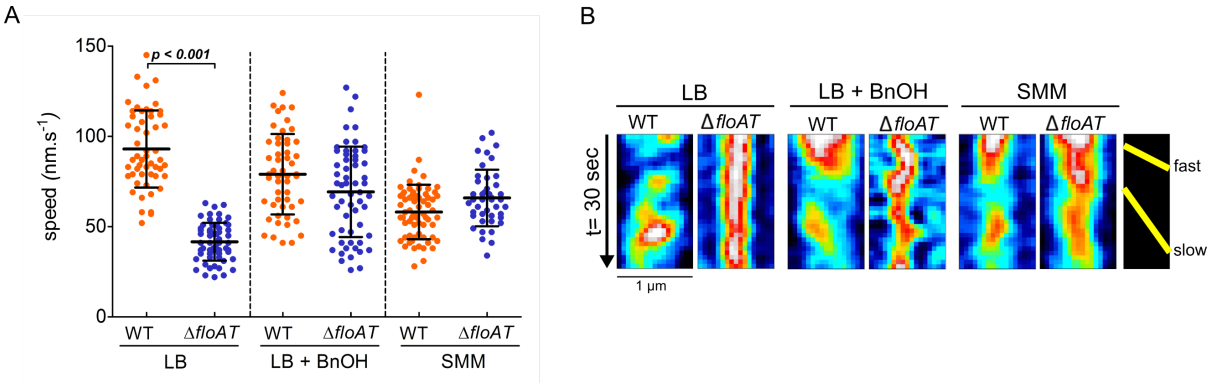

Figure 4. MreB speed is linked to membrane fluidity. (A) The MreB speed in different strain backgrounds and growth conditions was analysed by time-lapse TIRF microscopy. Scatter plot of the speed of patches obtained from individual tracks in 5 different cells are represented per fusion and condition. Average speeds are shown; error bars indicate the standard deviation. Significant statistical differences according to Dunn's multiple comparison tests after Kruskal–Wallis are represented ($p < 0.001$). **(B)** Representative kymographs showing fast and slow patches of mRFPruby-MreB in*B. subtilis* cells lacking endogenous *mreB* (WT) or *mreB* and *floAT* (Δ*floAT*). See supplementary movies S1-S6 for corresponding raw image series.

Flotillin increases fluidity of model membranes in vitro.

To assess whether the influence of flotillins on membrane fluidity is direct, we determined the membrane fluidity of model membranes with purified flotillin using solid-state NMR (ssNMR). ^{2}H ssNMR is a biophysical tool that assesses lipid mobility in native-like model membranes on the atomic level, by monitoring the carbon-deuterium order parameter of a deuterated lipid along the acyl chain (here POPC-d31)[41,42]. We purified *B. subtilis* FloT and tested the impact of FloT on the membrane, when reconstituted in POPC-d31 liposomes (schematically depicted in Figure 5B). FloT decreases the spectral width of the ^{2}H quadrupolar splitting, reflecting an increase in motion on the atomic scale (**Figure 5A**). The ^{2}H spectrum encodes the local order parameter S_{CD} of the carbon-deuterium in absence and in presence of FloT. Strikingly, FloT has an important impact on the order parameter along the entire acyl chain. It is remarkable that the protein significantly decreases the order parameter S_{CD}, reaching

252 even the inner carbon atoms of the acyl chain, indicating a different packing behavior and
253 increased membrane fluidity upon interaction with FloT (**Figure 5B**). The strong fluidizing
254 effect described for FloT is notably different from the effects other proteins have when
255 reconstituted into liposomes, such as plant remorins[42] or the membrane binding peptide of the
256 nonreceptor tyrosine kinase Src [43]. The anisotropic lineshape of the ^{31}P spectra indicates that
257 the membrane is in the lamellar phase as expected for POPC at the chosen temperature
258 (298K)[44]. Upon interactions with FloT the lamellar phase remains intact with formation of a
259 few smaller objects, indicating that the overall liposome structure is not affected and that its
260 phase is maintained (**Figure 5 figure supplement 1**).
261

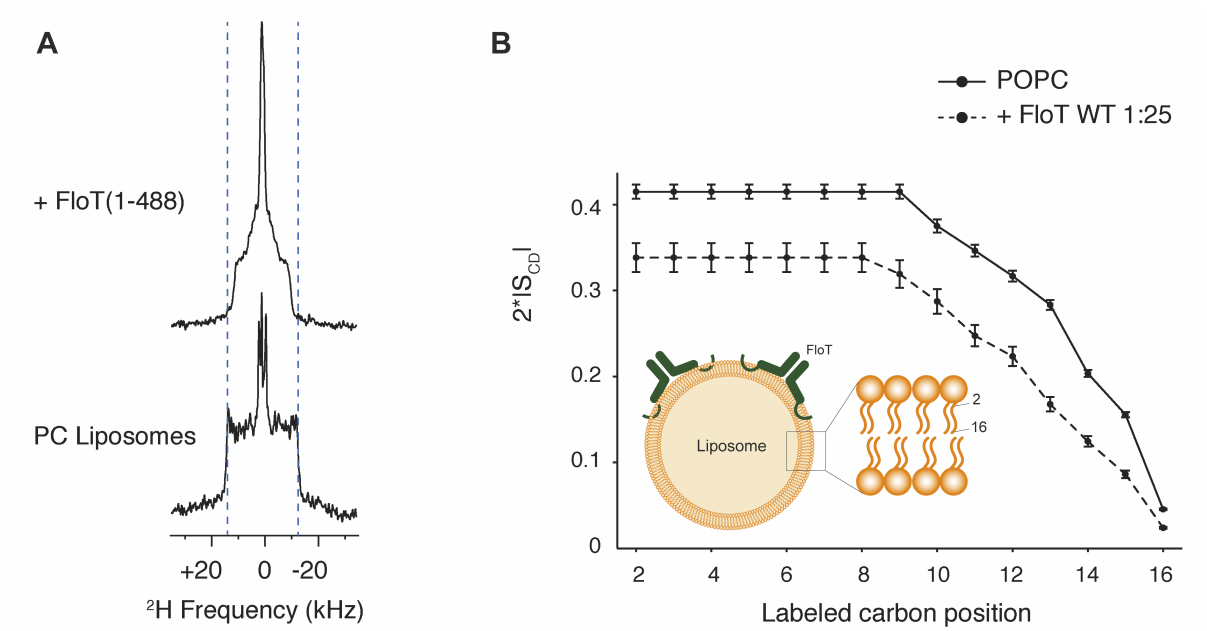

262

263 **Figure 5.** Lipid ordering of FloT probed by ^{2}H solid-state NMR. **(A)** Wide-line ^{2}H spectra of
264 POPC-d31 liposomes with or without FloT at a lipid-to-protein molar ratio of 25:1 acquired at
265 298 K. **(B)** Effect of FloT on the C-^{2}H order parameters of the PC acyl chain. De-Pake-ing and
266 simulations were applied on the ^{2}H solid-state NMR spectra to determine accurately individual
267 quadrupolar splittings. Order parameters of POPC-d31 acyl chain were derived from
268 experimental quadrupolar splittings and plotted as a function of the labeled carbon position.

269 *Insert:* schematic depiction of a liposome with added FloT which attaches to the membrane via
270 a hairpin loop[45].
271
272 **Discussion**

273 Our data provide evidence that flotillins play a direct role in controlling membrane fluidity and
274 that membrane fluidity is critical for peptidoglycan synthesis at certain growth conditions. *In*
275 *vitro*, flotillins enhance the fluidity of a model membrane, and *in vivo*, the membranes of fast
276 growing flotillin-mutant cells are less fluid even though the fatty acid composition in these
277 cells is identical. Therefore, we propose that the effect of flotillins on membrane fluidity is
278 direct, through a change in the packing behaviour of the lipids resulting in an efficient
279 separation of states of liquid ordered and disordered lipid domains in the membrane bilayer[24].
280 We found that membrane fluidity is not solely a function of temperature, but also of growth
281 conditions. *In vivo*, flotillins may also recruit specific, more rigid lipids, such as hopanoids and
282 carotenoids[18,20,21] which have been found in association with FMMs, and whose synthesis
283 could be growth condition dependent. The predominantly physical role in membrane
284 organization for flotillins fits with our observation that adding a chemical fluidizer is sufficient
285 to restore MreB dynamics and cell shape to fast growing cells that lack flotillins. We propose
286 that in fast-growing cells on rich medium, flotillin-mediated control of membrane fluidity is
287 critical and sufficient to allow essential membrane bound processes, such as peptidoglycan
288 synthesis, to proceed normally.

289 A sufficiently fluid membrane is necessary for the efficient recruitment and movement of
290 MreB, and provides a more favorable environment for the peptidoglycan precursor LipidII[8,9,17].
291 It has recently been shown that modulation of either MreBCD or PBP1 levels is sufficient to
292 alter the shape of *B. subtilis* cells[46], underscoring the importance of both systems. In the

293 absence of flotillins, the activity of the MreBCD component is strongly reduced – as evidenced
294 by the reduction of MreB speed – and the overall rigidity of the membrane is increased. This
295 results in a less favourable environment for the peptidoglycan precursor LipidII, which prefers
296 more liquid, disordered membrane phases[14,15,47]. Our data indicate that the reduction in
297 elongasome activity, which does not impact the growth rate itself, is compensated by increased
298 peptidoglycan synthesis activity around division sites in flotillin mutants, which is sufficient
299 to keep the overall cell shape intact, although cells are elongated. The accumulation of lipid
300 dyes indicative of increased fluidity at division sites is in line with a recent study that showed
301 phases of different fluidity in *Streptococcus pneumoniae* membranes, with more fluid
302 membranes and LipidII localizing at midcell[47] where the membrane is most bent. Our findings
303 are also in agreement with the recent observation that *B. subtilis* cells elongate and lose
304 organization of MreB when membrane fluidity is decreased by altering the membrane fatty
305 acid composition[48] (H. Strahl, personal communication). It could very well be that the shift of
306 fluidity towards the septum is only relative as the overall fluidity of the membrane is decreased
307 in the absence of flotillins. This is yet to be determined, as the resolution of Laurdan imaging
308 does not allow conclusive statements about local fluidity changes at the septum. It may seem
309 paradoxical that cells elongate when elongasome activity is reduced, but one has to remember
310 that a large amount of the peptidoglycan synthesis contributing to elongation of bacterial cells
311 is actually taking place at midcell, before the ingrowth of the septum[49-51]. The increased
312 peptidoglycan synthesis at future division sites makes the activity of PBP1 critical and explains
313 why its deletion has such a dramatic effect in cells lacking flotillins. Restoring fluidity using a
314 chemical fluidizer allows the MreBCD component to again efficiently drive peptidoglycan
315 synthesis during elongation, which is sufficient to suppress the flotillin mutant phenotype. The
316 net effect of this is that cells lacking PBP1 and flotillins grown with benzyl alcohol behave as
317 cells that only lack PBP1, which is quite similar to wild type. At low growth rates, there is no

318 difference between wild type cells and cells lacking flotillins with respect to membrane fluidity,
319 and the speed of MreB is similar between the two cell types. Thus, the deletion of flotillins
320 does not exacerbate the phenotype of cells lacking PBP1. The reason for the change in
321 membrane fluidity between cells grown on rich or minimal medium is not yet clear – it does
322 not seem to be caused by a large shift in the fatty acid composition of the membranes. Various
323 factors could play a role, such as the synthesis of specific lipids (hopanoids, isoprenoids) on
324 either type of medium, but also protein crowding, which is higher in membranes of fast-
325 growing cells than in slow-growing cells[52]. It will be an important future challenge to establish
326 the cause for this difference. An overall rigidification of the membrane may also lead to
327 retardation of processes which require membrane modifications such as division and
328 sporulation, which is indeed observed in *B. subtilis* flotillin mutants[25,53].
329 One of the proposed roles for flotillin proteins is that they form a 'platform' that transiently
330 interacts with membrane proteins that need to oligomerize into functional complexes[19]. We
331 tested this hypothesis for *B. subtilis* PBPs by comparing their localization and oligomerization
332 in wild type and flotillin mutant strains. Although we were capable of detecting a high MW
333 complex containing various PBPs (notably PBP1, 2a, 2b, 3 and 4), the complex was not
334 dependent on the presence of flotillins. We also note that PBP1 was present in the complex, as
335 well as present in a large smear in the first dimension native gel, which would explain why
336 PBP1 was detected by mass spectrometry analysis of a native PAGE band containing FloA[27].
337 PBP5, on the other hand, was not part of the high MW complex, which fits with its role in
338 processing of the terminal D-Ala from stem-peptides that have not been cross-linked, which it
339 exercises over the entire surface of the cell[32]. Although we cannot exclude that flotillins may
340 affect PBPs that are not easily detected by Bocillin-FL, our results do not provide any evidence
341 for a role for flotillins in the oligomerization of PBPs in *B. subtilis*. This extends the finding of
342 the Graumann lab that found either transient or no colocalization between flotillins and other

343 proteins present in DRM fractions[30]. Although it is obvious that peptidoglycan synthesis is
344 altered in the absence of flotillins, our data strongly suggest that the basis for this alteration is
345 in the physical organisation of the membrane rather than inefficient formation of divisome or
346 elongasome complexes in the absence of flotillins, because flotillin mutants strains show no
347 synthetic phenotype on minimal medium, and the defects on rich medium can be reverted by
348 chemically fluidizing the membrane.

349 In conclusion, our data provide a new model for flotillin function in the physical organization
350 of membranes during fast growth. The observation that flotillins differentially affect the
351 membrane in different growth conditions also explains the diversity of phenotypes described
352 for flotillin mutants in the literature.
353
354 **Methods**
355
356 *B. subtilis strains and growth conditions*
357 All *B. subtilis* strains used in this study are derived from strain 168 and are listed in **Table 1**.
358 Construction of new strains was based on natural competence of *B. subtilis*[54]. Gene integration
359 or deletion was validated by colony PCR whereas the expression and localization of the
360 fluorescent fusions was additionally validated by microscopy. Cells were grown either in LB
361 Lennox (5 g/L yeast extract; 5 g/L NaCl; 10 g/L tryptone)[55] or Spizizen minimal medium
362 (SMM)[56] supplemented with 1% glucose, at 37°C and 200 rpm, unless indicated otherwise.
363 Induction of the P_{xyl} promoter was triggered by addition of 0.2 - 0.5 % xylose. Cell cultures
364 were supplemented with spectinomycin (50 µg/ml), tetracycline (10 µg/ml), chloramphenicol
365 (5 µg/ml), kanamycin (5 µg/ml), erythromycin (1 µg/ml), benzyl alcohol (BnOH, 0.1 %) or
366 magnesium sulphate ($MgSO_4$, 6-20 mM) when necessary.
367

368 *Growth curves*

369 Growth experiments were performed either manually or automatically with a PowerWave 340
370 microplate reader (BioTek® Instruments, U.S.A). Strains were pre-cultured overnight in 3 ml
371 LB or SMM medium at 37 °C with shaking at 200 rpm. Next, stationary or late-exponentially
372 cells were diluted with fresh LB or SMM medium (supplemented when necessary), and cell
373 densities (OD_{600}) were measured every 1 hour when monitored manually or every 10 min when
374 monitored automatically, for a total time of 7-22 hours.

375

376 *Fluorescence microscopy*

377 For standard fluorescence microscopy, exponentially growing cells were immobilized on
378 microscope slides covered with a thin film of 1 % agarose (w/v) in water or the appropriate
379 medium. For TIRFM, agarose pads were mounted using Gene Frames (1.7 x 2.8 cm chamber,
380 0.25 mm thickness, 125 µL volume) from ThermoScientific. Standard fluorescence
381 microscopy was carried out using an Axio Zeiss Imager M1 fluorescence microscope (EC Plan-
382 Neofluar 100x/1.30 Oil Ph3 objective) equipped with an AxioCam HRm camera and an Nikon-
383 Ti-E microscope (Nikon Instruments, Tokyo, Japan) equipped with Hamamatsu Orca Flash 4.0
384 camera.

385 For Laurdan and TIRFM experiments, a Delta Vision Elite microscope (Applied Precision, GE
386 Healthcare) equipped with an Insight SSI™ Illumination, an X4 Laser module, a CoolSnap
387 HQ^2 CCD camera and a temperature-controlled chamber set up at 37 ^{0}C was used. Laurdan
388 images were taken with an Olympus UplanSApo 100x/1.4 oil objective. TIRFM image series
389 were taken using an Olympus UAPO N 100X/1.49 TIRF objective and a 561 nm laser (50 mW,
390 100 % power). Data processing was performed with softWoRx Suite 2.0 Software.

391

392 *Visualization of cell wall synthesis*

393 Peptidoglycan (PG) synthesis was assessed by labelling the cells with HADA (7-
394 hydroxycoumarin 3-carboxylic acid-amino-D-alanine)[57], Van-FL[33] or D-Ala-D-Pra[38].
395 HADA: synthesized as described[34]. Overnight cultures of *B. subtilis* strains were diluted 1:100
396 into fresh LB medium or LB medium supplemented with 0.1 % (w/v) of benzyl alcohol
397 (BnOH), a membrane fluidizer. Cells were grown until exponential phase, a sample of 1 ml of
398 culture was spun down for 30 sec, 5000 × g and the cell pellet was resuspended in 25 µl of
399 fresh pre-warmed LB or LB containing 0.1% (w/v) BnOH. HADA was added to a 50 µM final
400 concentration. Cells were incubated for 10 min in the dark (37 ^{0}C, 200 rpm) and then washed
401 twice in 1 ml PBS buffer (58 mM Na_2HPO_4, 17 mM NaH_2PO_4, 68 mM NaCl, pH 7.3) to remove
402 the excess of unbounded HADA. Cells were spun down again and resuspended in 25 µl of the
403 appropriate medium and 2 µl of cells were mounted on 1% agarose slides before visualization.
404 Visualization of HADA patterns (excitation: 358 nm/emission: 461 nm) under fluorescence
405 microscopy from two biological replicates and cell length measurements were taken from at
406 least 100 cells each strain/treatment.
407 Van-FL: a 1:1 mixture of vancomycin (Sigma Aldrich) and BODIPY®FL Vancomycin
408 (Molecular Probes) at a final concentration 1 µg/ml was used to label cells for 5-10 min at room
409 temperature.
410 D-Ala-D-Pra: synthesized as described[38]. 1 ml of cell cultures was pelleted and resuspended in
411 50 µl of PBS buffer. Dipeptide was added to a final concentration of 0.5 mM following with 5
412 min incubation at room temperature. Cells were fixed by adding 70 % ethanol and incubated
413 for minimum 2h in -20 °C. Next, cells were washed twice with PBS in order to remove
414 unattached peptides, and resuspended in 50 µl of PBS. The D-Ala-D-Pra was subsequently
415 labelled via a click reaction with fluorescent azide (20 µM) that was incubated for 15 min at
416 room temperature with addition of copper sulphate (CuSO4, 1 mM), tris-

417 hydroxypropyltriazolylmethylamine (THPTA, 125 µM) and ascorbic acid (1.2 mM). The
418 sample was washed twice with PBS and resuspended in 50 µl of the same buffer.
419
420 *Laurdan staining and GP calculations*
421 Laurdan (6-Dodecanoyl-N, N-dymethyl2-naphthylamine, Sigma-Aldrich) was used to detect
422 the liquid ordering in the membrane, as decribed[24], with modifications. Cells were grown in
423 LB or SMM medium until late exponential phase. Laurdan, dissolved in dimethyformamide
424 (DMF), was added at 10 µM final concentration and cells were incubated for 10 min in the
425 dark at 37 ^{0}C, 200 rpm. Cells were then washed twice in PBS buffer supplemented with 0.2 %
426 (w/v) glucose and 1% (w/v) DMF, and resuspended in fresh prewarmed appropriate medium.
427 Laurdan was excited at 360 ± 20 nm, and fluorescence emission was captured at 460 ± 25 nm
428 (exposure time: 500 ms) and at 535 ± 25 nm (exposure time: 1 sec)[13]. The image analysis
429 including the generation of GP maps was carried out using Fiji Software[58] in combination with
430 the macro tool CalculateGP designed by Norbert Vischer
431 (http://sils.fnwi.uva.nl/bcb/objectj/examples/CalculateGP/MD/gp.html). The GP values were
432 measured for at least 100 individual cells after background subtraction, from two biological
433 replicates.
434
435 *Other fluorescent membrane probes*
436 *B. subtilis* cell membranes were probed with Nile Red (0.5 µg.ml^{-1}), FM4-64 (0.5 µg.ml^{-1}) or
437 DiI-C12 (2.5 µg.ml^{-1}). To this end, an overnight culture was grown in appropriate antibiotic,
438 diluted 1:100 in LB medium supplemented with DiI-C12 followed by growth until exponential
439 phase. Membranes were probed with Nile Red or FM4-64 for 5 min at room temperature after
440 reaching exponential phase. The stained cells were washed three times in prewarmed LB
441 medium supplemented with 1 % DMSO before visualization under fluorescence microscopy.

442

443 *TIRF time lapse microscopy*

444 Time-lapse TIRFM movies were taken in two independent experiments for each strain and
445 condition. To this end, overnight cultures of strains grown in LB medium supplemented with
446 the appropriate antibiotic were diluted 1:100 in medium containing 0.5 % (w/v) xylose and
447 grown until exponential phase. All experiments were performed inside the incubation chamber
448 set to 37 ^{0}C, no longer than 10 min after taking the sample. The cells were imaged over 30 s
449 with 1 s inter-frame intervals in a continuous illumination and ultimate focus correction mode.
450 The single particle tracking analyses and kymographs were done using Fiji Software[58] in
451 combination with the MTrackJ[59] and MicrobeJ plugins[60].

452

453 *Bocillin labelling*

454 Cells were grown until an OD600 of 0.4 - 0.5, and washed twice with PBS. Next, samples were
455 resuspended in 50 µl PBS containing Bocillin-FL (5 µg.ml^{-1}) and incubated at room
456 temperature for 10 min. Subsequently cells were harvested, lysed by sonication and cell-free
457 extracts were prepared. Samples, equalized for culture OD, were prepared with SDS-PAGE
458 sample buffer and run on a 12 % SDS-PAGE gel. Fluorescent bands were visualized using a
459 Typhoon Trio (GE Healthcare) scanner.

460

461 *Isolation of membranes*

462 Membrane isolation was adapted from[61]. Briefly, cells were grown until an OD600 of 0.4 - 0.5,
463 cell fractions were collected and resuspended in PBS with Lysozyme (1 µg.ml^{-1}), EDTA (5
464 mM), 1/10 tablet cOmplete protease inhibitor (Roche), and DNAse (5 µg.ml^{-1}) and incubated
465 for 30 min on ice. Samples were sonicated, cell which did not lyze were spun down (8000 rpm,
466 2 min, 4°C), and the supernatant fraction was centrifuged at 4°C and 40000 rpm for 1 h. The

467 membrane pellet was dissolved in ACA750 buffer (750 mM aminocaproic acid, 50 mM Bis-
468 Tris, pH 7.0) to a final protein concentration of 1 µg/µl. Membranes were solubilized overnight
469 at 4°C in 1 % (w/v) dodecylmaltoside (DDM) and either used directly or stored at -20°C.
470
471 *Blue native PAGE (BN-PAGE)*
472 The experiment was performed as described[36]. Samples were prepared by mixing sample buffer
473 (0.1 % Ponceau S, 42.5 % Glycerol) with solubilized membranes in a 1:3 ratio. Samples were
474 resolved on a mini-PROTEAN™ TGX Stain-Free™ gradient gel (4-15%, BioRad) using
475 cathode (50 mM Tricine and 15 mM BisTris), and anode (50 mM BisTris pH 7.0) buffers. The
476 Novex® NativeMark™ Unstained Protein Standard® marker was used as a Mw marker.
477
478 *Second dimension SDS PAGE (2D SDS-PAGE)*
479 A lane of interest was excised from the Native-PAGE gel and immobilized horizontally on top
480 of a SDS-PAGE gel (5% stacking, 12% resolving). The excised fragment was flanked with a
481 piece of Whatman™ paper soaked with PageRuler™ Prestained Protein Ladder. The gel
482 fragment to be resolved in the second dimension was topped with a mix of 1 % (w/v)
483 LowTemperature agarose, 0.5 % (w/v) SDS and bromophenol blue. After the agarose had
484 solidified, standard SDS-PAGE electrophoresis was performed.
485
486 *TEM*
487 Cultures were harvested by centrifugation and a small amount of pellet was placed on a copper
488 dish. A 400 copper mesh grid and a 75 µm aperture grid was placed on top of the cells to create
489 a thin layer. The sandwiched cells were plunged rapidly into liquid propane. Sandwiches were
490 then disassembled and placed on frozen freeze-substitution medium containing 1 % osmium
491 tetroxide, 0.5 % uranyl acetate and 5 % water in acetone. Cells were dehydrated and fixed using

492 the rapid freeze substitution method[62]. Samples were embedded in epon and ultrathin sections
493 were collected on formvar coated and carbon evaporated copper grids and inspected using a
494 CM12 (Philips) transmission electron microscope. For each strain 70 random septa were
495 imaged with pixel resolution of 1.2 nm. Using ImageJ the cell wall thickness for each septum
496 was measured at 4 places from which the average was taken.
497
498 *Statistical Analysis*
499 Each set of micrographs to be analysed was imaged with the same exposure time. For the
500 septum intensity analysis of HADA, FM4-64 and Nile Red, the wildtype strain (expressing
501 GFP) and the Δ*floAT strains* were mixed, labelled and imaged on the same agarose pad.
502 Intensity of the fluorescently labelled septa was measured using the ObjectJ macro tool
503 PeakFinder (https://sils.fnwi.uva.nl/bcb/objectj/examples/PeakFinder/peakfinder.html)[63]. A
504 perpendicular line was drawn across the septal plane, the background intensity was removed
505 resulting in a maximum peak intensity. The number of septa compared was indicated for every
506 individual experiment. Populations were compared using the non-parametric Mann-Whitney
507 test. The null hypothesis was tested with the p value of 0.05. The statistical analyses and their
508 graphical representation (box plots) were generated with GraphPad Prism 8.1 (San Diego,
509 California, USA). Box plots show the median and the interquartile range (box), the 5th and
510 95th percentile (whiskers). Laurdan fluorescence generalized polarization, cell length and
511 MreB speed statistical analyses were performed using Kruskal-Wallis with Dunn's multiple
512 comparison *post-hoc* test.
513
514 *Fatty acid composition analysis*

515 The fatty acid composition of *B. subtilis* wild-type cells and the flotillin/PBP mutants was
516 analyzed with gas chromatography as fatty acid methyl esters. Cells for the analyses were
517 grown at 37 °C in LB or SMM until mid-exponential (OD_{600} ~ 0.5), harvested (6000 rpm, 10
518 min, 4 °C) and washed with 100 mM NaCl. Next, the cells were freeze dried at -50 ºC, 0.012
519 mbar for a minimum of 18 h. All analyses were carried out on biological duplicates by the
520 Identification Service of the DSMZ, Braunschweig, Germany.
521
522 *Sample preparation for solid-state NMR*
523 FloT was essentially purified as described[24], in solubilized form, and stored in buffer A (50
524 mM Tris HCl pH 7.5, 150 mM NaCl, 5 mM $MgCl_2$) supplemented with 0.05 % Triton X-100.
525 Liposomes containing POPC-d31 were prepared by mixing appropriate lipid powders in
526 organic solvents (chloroform/methanol, 2:1 ratio). Solvents were evaporated under a flow of
527 N_2 to obtain a thin lipid film. Lipids were rehydrated with ultrapure water before lyophilisation
528 over night. The lipid powder was hydrated with an appropriate amount of buffer A with 10%
529 glycerol and homogenized by three cycles of vortexing, freezing (liquid nitrogen, -196°C, 1
530 min) and thawing (40°C in a water bath, 10 min). This protocol generated a milky suspension
531 of micrometer-sized multilamellar vesicles. FloT was solubilized in Buffer A supplemented
532 with 0.05% Triton X-100 and added to preformed liposomes and incubated for 1h at room
533 temperature. A dialysis step was then performed against Buffer A at 4°C under agitation to
534 remove the detergent. Samples were centrifuged at 100,000g at 4°C for 1h to pellet the
535 proteoliposomes. ^2H solid-state NMR spectra were recorded of liposomes in the presence or
536 absence of FloT at a lipid/protein ratio of 25:1 at 298 K.
537
538 *Solid-state NMR*

539 ^{2}H NMR spectroscopy experiments were performed using a Bruker Avance III 500 MHz WB
540 (11.75 T) spectrometer. They were recorded on ^{2}H-labeled POPC at 76.77 MHz with a phase-
541 cycled quadrupolar echo pulse sequence (90°x-t-90°y-t-acq). Acquisition parameters were as
542 follows: spectral window of 500 kHz for 2H NMR spectroscopy, p/2 pulse width of 3.90 ms
543 for ^{2}H, interpulse delays (t) were of 40 µs, recycled delays of 1.3 s for 2H; 3000 and 8000 scans
544 were used for ^{2}H NMR spectroscopy on liposomes and liposomes with FloT, respectively.
545 Spectra were processed using a Lorentzian line broadening of 300 Hz for ^{2}H NMR spectra
546 before Fourier transformation from the top of the echo. Samples were equilibrated for 30 min
547 at a given temperature before data acquisition. All spectra were processed and analyzed using
548 Bruker Topspin 3.2 software. Spectral moments were calculated for each temperature using the
549 NMR Depaker 1.0rc1 software [Copyright (C) 2009 Sébastien Buchoux]. Orientational order
550 parameters (SCD) were calculated from experimental quadrupolar splittings (DnQ) as
551 described in Huster 2014. For ^{31}P ssNMR, we applied a static Hahn spin echo sequence at the
552 ^{31}P frequency of 162 MHz on a 400 MHz (9.4T) Bruker Avance III HD spectrometer, with a
553 90◦ pulse of 8 µs, a delay of 40 µs, a recycle delay of 5 s, a spectral window of 400 ppm and a
554 number of scans of 4000 and 3400 was used on liposomes and liposomes with FloT,
555 respectively. Spectra were processed using a Lorentzian line broadening of 100 Hz.
556

557 **Acknowledgements:**

558 We thank Henrik Strahl for discussions and sharing of unpublished data, Rut Carballido-Lopez
559 for strain RWBS5 and Luiza Morawska and Oscar Kuipers for the P*rrnB-gfp* plasmid.
560 This work was funded by NWO grant 864.09.010 (DJS), DFG grants BR 2915/4-1; INST
561 86/1452-1 (MB), ERC starting grant 757913; NWO grant 721.014.008 (AKHH); PhD
562 fellowships DAAD-GSSP to AS; and SFRH/BD/78061/2011- POPH/FSE/FCT to ASB.

563 **Contributions:**

564 AZ, AS, ASB, BH, MBr, DJS designed experiments. AZ, AS, ASB, MBe, DM, JR, RB
565 performed experiments. AZ, AS, ASB, MBe, DM, JR, RB, IK, BH, MBr, DJS analysed
566 experiments. AH, AKHH contributed reagents. AZ, AS, BH, MBr, DJS wrote the manuscript,
567 all authors read and commented on the manuscript.

568

569 **Competing interests**

570 The authors declare that they have no competing interests.

571

572 **References**

573 1 Typas, A., Banzhaf, M., Gross, C. A. & Vollmer, W. From the regulation of
574 peptidoglycan synthesis to bacterial growth and morphology. *Nat Rev Microbiol* **10**,
575 123-136, doi:10.1038/nrmicro2677 (2012).
576 2 Zhao, H., Patel, V., Helmann, J. D. & Dorr, T. Don't let sleeping dogmas lie: new views
577 of peptidoglycan synthesis and its regulation. *Mol Microbiol* **106**, 847-860,
578 doi:10.1111/mmi.13853 (2017).
579 3 Cho, H. *et al.* Bacterial cell wall biogenesis is mediated by SEDS and PBP polymerase
580 families functioning semi-autonomously. *Nat Microbiol*, 16172,
581 doi:10.1038/nmicrobiol.2016.172 (2016).
582 4 Meeske, A. J. *et al.* SEDS proteins are a widespread family of bacterial cell wall
583 polymerases. *Nature* **537**, 634-638, doi:10.1038/nature19331 (2016).
584 5 Taguchi, A. *et al.* FtsW is a peptidoglycan polymerase that is functional only in
585 complex with its cognate penicillin-binding protein. *Nat Microbiol*,
586 doi:10.1038/s41564-018-0345-x (2019).
587 6 Morales Angeles, D. & Scheffers, D. J. in *Bacillus: Cellular and Molecular Biology* (ed
588 P. L. Graumann) Ch. 10, 295-332 (Caister Academic Press, U.K., 2017).
589 7 Strahl, H. & Errington, J. Bacterial Membranes: Structure, Domains, and Function.
590 *Annual Review of Microbiology* **71**, 519-538, doi:10.1146/annurev-micro-102215-
591 095630 (2017).
592 8 Hussain, S. *et al.* MreB filaments align along greatest principal membrane curvature
593 to orient cell wall synthesis. *eLife* **7**, doi:10.7554/eLife.32471 (2018).
594 9 Ursell, T. S. *et al.* Rod-like bacterial shape is maintained by feedback between cell
595 curvature and cytoskeletal localization. *Proc Natl Acad Sci U S A* **111**, E1025-1034,
596 doi:10.1073/pnas.1317174111 (2014).
597 10 Dominguez-Escobar, J. *et al.* Processive movement of MreB-associated cell wall
598 biosynthetic complexes in bacteria. *Science* **333**, 225-228,
599 doi:10.1126/science.1203466 (2011).
600 11 Garner, E. C. *et al.* Coupled, circumferential motions of the cell wall synthesis
601 machinery and MreB filaments in B. subtilis. *Science* **333**, 222-225,
602 doi:10.1126/science.1203285 (2011).

603 12 Billaudeau, C. *et al.* Contrasting mechanisms of growth in two model rod-shaped
604 bacteria. *Nat Commun* **8**, 15370, doi:10.1038/ncomms15370 (2017).
605 13 Strahl, H., Burmann, F. & Hamoen, L. W. The actin homologue MreB organizes the
606 bacterial cell membrane. *Nat Commun* **5**, 3442, doi:10.1038/ncomms4442 (2014).
607 14 Ganchev, D. N., Hasper, H. E., Breukink, E. & de Kruijff, B. Size and orientation of the
608 lipid II headgroup as revealed by AFM imaging. *Biochemistry* **45**, 6195-6202,
609 doi:10.1021/bi051913e (2006).
610 15 Witzke, S., Petersen, M., Carpenter, T. S. & Khalid, S. Molecular Dynamics
611 Simulations Reveal the Conformational Flexibility of Lipid II and Its Loose Association
612 with the Defensin Plectasin in the Staphylococcus aureus Membrane. *Biochemistry*
613 **55**, 3303-3314, doi:10.1021/acs.biochem.5b01315 (2016).
614 16 Muchova, K., Wilkinson, A. J. & Barak, I. Changes of lipid domains in Bacillus subtilis
615 cells with disrupted cell wall peptidoglycan. *FEMS Microbiol Lett* **325**, 92-98,
616 doi:10.1111/j.1574-6968.2011.02417.x (2011).
617 17 Schirner, K. *et al.* Lipid-linked cell wall precursors regulate membrane association of
618 bacterial actin MreB. *Nat Chem Biol* **11**, 38-45, doi:10.1038/nchembio.1689 (2015).
619 18 Bramkamp, M. & Lopez, D. Exploring the existence of lipid rafts in bacteria. *Microbiol*
620 *Mol Biol Rev* **79**, 81-100, doi:10.1128/MMBR.00036-14 (2015).
621 19 Lopez, D. & Koch, G. Exploring functional membrane microdomains in bacteria: an
622 overview. *Current Opinion in Microbiology* **36**, 76 - 84,
623 doi:https://doi.org/10.1016/j.mib.2017.02.001 (2017).
624 20 García-Fernández, E. *et al.* Membrane Microdomain Disassembly Inhibits MRSA
625 Antibiotic Resistance. *Cell* **171**, 1354-1367.e1320, doi:10.1016/j.cell.2017.10.012
626 (2017).
627 21 Lopez, D. & Kolter, R. Functional microdomains in bacterial membranes. *Genes Dev*
628 **24**, 1893-1902, doi:10.1101/gad.1945010 (2010).
629 22 Mielich-Suss, B. & Lopez, D. Molecular mechanisms involved in Bacillus subtilis
630 biofilm formation. *Environmental microbiology* **17**, 555-565, doi:10.1111/1462-
631 2920.12527 (2015).
632 23 Mielich-Suss, B., Schneider, J. & Lopez, D. Overproduction of flotillin influences cell
633 differentiation and shape in Bacillus subtilis. *mBio* **4**, e00719-00713,
634 doi:10.1128/mBio.00719-13 (2013).
635 24 Bach, J. N. & Bramkamp, M. Flotillins functionally organize the bacterial membrane.
636 *Mol Microbiol* **88**, 1205-1217, doi:10.1111/mmi.12252 (2013).
637 25 Dempwolff, F., Moller, H. M. & Graumann, P. L. Synthetic motility and cell shape
638 defects associated with deletions of flotillin/reggie paralogs in Bacillus subtilis and
639 interplay of these proteins with NfeD proteins. *J Bacteriol* **194**, 4652-4661,
640 doi:10.1128/JB.00910-12 (2012).
641 26 Yepes, A. *et al.* The biofilm formation defect of a Bacillus subtilis flotillin-defective
642 mutant involves the protease FtsH. *Mol Microbiol* **86**, 457-471, doi:10.1111/j.1365-
643 2958.2012.08205.x (2012).
644 27 Schneider, J. *et al.* Spatio-temporal remodeling of functional membrane
645 microdomains organizes the signaling networks of a bacterium. *PLoS genetics* **11**,
646 e1005140, doi:10.1371/journal.pgen.1005140 (2015).
647 28 Huang, X., Gaballa, A., Cao, M. & Helmann, J. D. Identification of target promoters
648 for the Bacillus subtilis extracytoplasmic function sigma factor, sigma W. *Mol*
649 *Microbiol* **31**, 361-371 (1999).

650 29 Nicolas, P. *et al.* Condition-dependent transcriptome reveals high-level regulatory
651 architecture in Bacillus subtilis. *Science* **335**, 1103-1106,
652 doi:10.1126/science.1206848 (2012).
653 30 Dempwolff, F. *et al.* Super Resolution Fluorescence Microscopy and Tracking of
654 Bacterial Flotillin (Reggie) Paralogs Provide Evidence for Defined-Sized Protein
655 Microdomains within the Bacterial Membrane but Absence of Clusters Containing
656 Detergent-Resistant Proteins. *PLoS genetics* **12**, e1006116,
657 doi:10.1371/journal.pgen.1006116 (2016).
658 31 Mielich-Suss, B. *et al.* Flotillin scaffold activity contributes to type VII secretion
659 system assembly in Staphylococcus aureus. *PLoS pathogens* **13**, e1006728,
660 doi:10.1371/journal.ppat.1006728 (2017).
661 32 Kuru, E. *et al.* In Situ probing of newly synthesized peptidoglycan in live bacteria with
662 fluorescent D-amino acids. *Angew Chem Int Ed Engl* **51**, 12519-12523,
663 doi:10.1002/anie.201206749 (2012).
664 33 Daniel, R. A. & Errington, J. Control of cell morphogenesis in bacteria: two distinct
665 ways to make a rod-shaped cell. *Cell* **113**, 767-776 (2003).
666 34 Morales Angeles, D. *et al.* Pentapeptide-rich peptidoglycan at the Bacillus subtilis
667 cell-division site. *Mol Microbiol* **104**, 319-333, doi:10.1111/mmi.13629 (2017).
668 35 Kahan, F. M., Kahan, J. S., Cassidy, P. J. & Kropp, H. The mechanism of action of
669 fosfomycin (phosphonomycin). *Ann N Y Acad Sci* **235**, 364-386, doi:10.1111/j.1749-
670 6632.1974.tb43277.x (1974).
671 36 Trip, E. N. & Scheffers, D. J. A 1 MDa protein complex containing critical components
672 of the Escherichia coli divisome. *Sci Rep* **5**, 18190, doi:10.1038/srep18190 (2015).
673 37 Scheffers, D. J. & Errington, J. PBP1 Is a Component of the Bacillus subtilis Cell
674 Division Machinery. *Journal of Bacteriology* **186**, 5153-5156 (2004).
675 38 Sarkar, S., Libby, E. A., Pidgeon, S. E., Dworkin, J. & Pires, M. M. In Vivo Probe of Lipid
676 II-Interacting Proteins. *Angew Chem Int Ed Engl* **55**, 8401-8404,
677 doi:10.1002/anie.201603441 (2016).
678 39 Dajkovic, A. *et al.* Hydrolysis of peptidoglycan is modulated by amidation of meso-
679 diaminopimelic acid and Mg(2+) in Bacillus subtilis. *Mol Microbiol* **104**, 972-988,
680 doi:10.1111/mmi.13673 (2017).
681 40 Konopasek, I., Strzalka, K. & Svobodova, J. Cold shock in Bacillus subtilis: different
682 effects of benzyl alcohol and ethanol on the membrane organisation and cell
683 adaptation. *Biochim Biophys Acta* **1464**, 18-26 (2000).
684 41 Molugu, T. R., Lee, S. & Brown, M. F. Concepts and Methods of Solid-State NMR
685 Spectroscopy Applied to Biomembranes. *Chemical Reviews* **117**, 12087-12132,
686 doi:10.1021/acs.chemrev.6b00619 (2017).
687 42 Legrand, A. *et al.* Nanodomain Clustering of the Plant Protein Remorin by Solid-State
688 NMR. *Frontiers in Molecular Biosciences* **6**, doi:10.3389/fmolb.2019.00107 (2019).
689 43 Scheidt, H. A. & Huster, D. Structure and Dynamics of the Myristoyl Lipid
690 Modification of Src Peptides Determined by 2H Solid-State NMR Spectroscopy.
691 *Biophysical Journal* **96**, 3663-3672, doi:https://doi.org/10.1016/j.bpj.2009.02.028
692 (2009).
693 44 Huster, D. Solid-state NMR spectroscopy to study protein–lipid interactions.
694 *Biochimica et Biophysica Acta (BBA) - Molecular and Cell Biology of Lipids* **1841**,
695 1146-1160, doi:https://doi.org/10.1016/j.bbalip.2013.12.002 (2014).

696 45 Bach, J. N. & Bramkamp, M. Dissecting the molecular properties of prokaryotic
697 flotillins. *PLoS One* **10**, e0116750, doi:10.1371/journal.pone.0116750 (2015).
698 46 Dion, M. F. *et al.* Bacillus subtilis cell diameter is determined by the opposing actions
699 of two distinct cell wall synthetic systems. *Nat Microbiol*, doi:10.1038/s41564-019-
700 0439-0 (2019).
701 47 Calvez, P., Jouhet, J., Vie, V., Durmort, C. & Zapun, A. Lipid Phases and Cell Geometry
702 During the Cell Cycle of Streptococcus pneumoniae. *Frontiers in microbiology* **10**,
703 351, doi:10.3389/fmicb.2019.00351 (2019).
704 48 Gohrbandt, M. *et al.* Low membrane fluidity triggers lipid phase separation and
705 protein segregation in vivo. *bioRxiv*, 852160, doi:10.1101/852160
706 (2019).
707 49 Pazos, M. *et al.* Z-ring membrane anchors associate with cell wall synthases to
708 initiate bacterial cell division. *Nat Commun* **9**, 5090, doi:10.1038/s41467-018-07559-
709 2 (2018).
710 50 Varma, A. & Young, K. D. In Escherichia coli, MreB and FtsZ direct the synthesis of
711 lateral cell wall via independent pathways that require PBP 2. *J Bacteriol* **191**, 3526-
712 3533, doi:10.1128/JB.01812-08 (2009).
713 51 Aaron, M. *et al.* The tubulin homologue FtsZ contributes to cell elongation by guiding
714 cell wall precursor synthesis in Caulobacter crescentus. *Molecular Microbiology* **64**,
715 938-952, doi:doi:10.1111/j.1365-2958.2007.05720.x (2007).
716 52 Szenk, M., Dill, K. A. & de Graff, A. M. R. Why Do Fast-Growing Bacteria Enter
717 Overflow Metabolism? Testing the Membrane Real Estate Hypothesis. *Cell Syst* **5**, 95-
718 104, doi:10.1016/j.cels.2017.06.005 (2017).
719 53 Donovan, C. & Bramkamp, M. Characterization and subcellular localization of a
720 bacterial flotillin homologue. *Microbiology* **155**, 1786-1799,
721 doi:10.1099/mic.0.025312-0 (2009).
722 54 Harwood, C. R. & Cutting, S. M. *Molecular Biological Methods for Bacillus*. (John
723 Wiley and Sons, 1990).
724 55 Lennox, E. S. Transduction of linked genetic characters of the host by bacteriophage
725 P1. *Virology* **1**, 190-206, doi:10.1016/0042-6822(55)90016-7 (1955).
726 56 Anagnostopoulos, C. & Spizizen, J. Requirements for transformation in Bacillus
727 subtilis. *Journal of Bacteriology* **81**, 741-746 (1961).
728 57 Kuru, E., Tekkam, S., Hall, E., Brun, Y. V. & Van Nieuwenhze, M. S. Synthesis of
729 fluorescent D-amino acids and their use for probing peptidoglycan synthesis and
730 bacterial growth in situ. *Nat Protoc* **10**, 33-52, doi:10.1038/nprot.2014.197 (2015).
731 58 Schindelin, J. *et al.* Fiji: an open-source platform for biological-image analysis. *Nat*
732 *Methods* **9**, 676-682, doi:10.1038/nmeth.2019 (2012).
733 59 Meijering, E., Dzyubachyk, O. & Smal, I. Methods for cell and particle tracking.
734 *Methods Enzymol* **504**, 183-200, doi:10.1016/B978-0-12-391857-4.00009-4 (2012).
735 60 Ducret, A., Quardokus, E. M. & Brun, Y. V. MicrobeJ, a tool for high throughput
736 bacterial cell detection and quantitative analysis. *Nat Microbiol* **1**, 16077,
737 doi:10.1038/nmicrobiol.2016.77 (2016).
738 61 Schneider, J., Mielich-Suss, B., Bohme, R. & Lopez, D. In vivo characterization of the
739 scaffold activity of flotillin on the membrane kinase KinC of Bacillus subtilis.
740 *Microbiology* **161**, 1871-1887, doi:10.1099/mic.0.000137 (2015).

741 62 McDonald, K. L. Out with the old and in with the new: rapid specimen preparation
742 procedures for electron microscopy of sectioned biological material. *Protoplasma*
743 **251**, 429-448, doi:10.1007/s00709-013-0575-y (2014).
744 63 Vischer, N. O. *et al.* Cell age dependent concentration of Escherichia coli divisome
745 proteins analyzed with ImageJ and ObjectJ. *Frontiers in microbiology* **6**, 586,
746 doi:10.3389/fmicb.2015.00586 (2015).
747 64 Scheffers, D.-J., Jones, L. J. F. & Errington, J. Several distinct localization patterns for
748 penicillin-binding proteins in Bacillus subtilis. *Mol Microbiol* **51**, 749-764 (2004).
749 65 Lages, M. C., Beilharz, K., Morales Angeles, D., Veening, J. W. & Scheffers, D. J. The
750 localization of key Bacillus subtilis penicillin binding proteins during cell growth is
751 determined by substrate availability. *Environmental microbiology* **15**, 3272-3281,
752 doi:10.1111/1462-2920.12206 (2013).
753 66 Veening, J. W., Murray, H. & Errington, J. A mechanism for cell cycle regulation of
754 sporulation initiation in Bacillus subtilis. *Genes Dev* **23**, 1959-1970,
755 doi:10.1101/gad.528209 (2009).
756

757

758

759

760 **Table 1. Strain list**

Strain	Genotype	Source
168	*trpC2*	Laboratory collection
BB001	*trpC2 yqfA::tet*	24
BB003	*trpC2 yuaG::pMUTIN4 yqfA::tet*	24
DB003	*trpC2 yuaG::pMUTIN4*	53
2082	*trpC2 pbpD::cat Pxyl–gfp–pbpD* $^{1–510}$	64
2083	*trpC2 ponA::cat Pxyl–gfp–ponA* $^{1–394}$	64
2085	*trpC2 dacA::cat Pxyl–gfp–dacA* $^{1–423}$	64
3105	*trpC2 pbpC::cat Pxyl–gfp–pbpC* $^{1–768}$	64
3122	*trpC2 pbpB::cat Pxyl-gfp-pbpB* $^{1–825}$	64
3511	*trpC2 ponA::spc*	37
4042	*trpC2 pbpA::cat Pxyl-mkate2-pbpA* $^{1–804}$	65
4056	*trpC2 dacA::kan*	34
RWBS 5	*amyE::spc Pxyl mrfpruby-mreB*	10
4059	*trpC2 dacA::cat Pxyl–gfp–dacA* $^{1–423}$ *yuaG::pMUTIN4 yqfA::tet*	This work
4064	*trpC2 dacA::kan yuaG::pMUTIN4 yqfA::tet*	This work
4090	*trpC2 ponA::spc yuaG::pMUTIN4*	This work
4091	*ponA::spc yqfA::tet*	This work
4092	*trpC2 ponA::spc yuaG::pMUTIN4 yqfA::tet*	This work
4095	*trpC2 ponA::cat Pxyl–gfp–ponA* $^{1–394}$ *yuaG::pMUTIN4 yqfA::tet*	This work

4099	*trpC2 pbpB::cat Pxyl-gfp-pbpB* $^{1–825}$ *yuaG::pMUTIN4 yqfA::tet*	This work
4102	*trpC2 pbpA::cat Pxyl-mkate2-pbpA* $^{1–804}$ *yuaG::pMUTIN4 yqfA::tet*	This work
4108	*trpC2 pbpD::cat Pxyl–gfp–pbpD* $^{1–510}$ *yuaG::pMUTIN4 yqfA::tet*	This work
4122	*trpC2 pbpC::cat Pxyl–gfp–pbpC* $^{1–768}$ *yuaG::pMUTIN4 yqfA::tet*	This work
4128	*trpC2 ponA::spc pbpD::cat Pxyl–gfp–pbpD* $^{1–510}$	This work
4129	*trpC2 ponA::spc yuaG::pMUTIN4 pbpD::cat Pxyl–gfp–pbpD* $^{1–510}$	This work
4070	*trpC2 mreB::kan amyE::spc Pxyl mrfpruby-mreB*	This work
4076	*trpC2 mreB::kan amyE::spc Pxyl mrfpruby-mreB yuaG::pMUTIN4 yqfA::tet*	This work
4259	*trpC2 amyE::*P_{rrnB}*-GFP*	This work, [66]

761